

Final work : Impact Damage Modelling on Composite Structures

Auteur : Jerez Sotoca, Irene

Promoteur(s) : Ponthot, Jean-Philippe

Faculté : Faculté des Sciences appliquées

Diplôme : Master en ingénieur civil en aérospatiale, à finalité spécialisée en "turbomachinery aeromechanics (THRUST)"

Année académique : 2022-2023

URI/URL : <http://hdl.handle.net/2268.2/18327>

Avertissement à l'attention des usagers :

Tous les documents placés en accès ouvert sur le site le site MatheO sont protégés par le droit d'auteur. Conformément aux principes énoncés par la "Budapest Open Access Initiative"(BOAI, 2002), l'utilisateur du site peut lire, télécharger, copier, transmettre, imprimer, chercher ou faire un lien vers le texte intégral de ces documents, les disséquer pour les indexer, s'en servir de données pour un logiciel, ou s'en servir à toute autre fin légale (ou prévue par la réglementation relative au droit d'auteur). Toute utilisation du document à des fins commerciales est strictement interdite.

Par ailleurs, l'utilisateur s'engage à respecter les droits moraux de l'auteur, principalement le droit à l'intégrité de l'oeuvre et le droit de paternité et ce dans toute utilisation que l'utilisateur entreprend. Ainsi, à titre d'exemple, lorsqu'il reproduira un document par extrait ou dans son intégralité, l'utilisateur citera de manière complète les sources telles que mentionnées ci-dessus. Toute utilisation non explicitement autorisée ci-avant (telle que par exemple, la modification du document ou son résumé) nécessite l'autorisation préalable et expresse des auteurs ou de leurs ayants droit.

Chapter 7

Appendix A: LS Dyna Specifications

7.1 Governing equations

It is important to understand which are the equations that the software aims to solve during the problem [43]. The main equations that govern the physical problem that is here to be solved are as follows:

- Momentum equation:

$$\sigma_{ij,j} + \rho f_i = \rho \ddot{x}_i, \quad (7.1)$$

where σ is the Cauchy stress tensor, ρ is the current density, \mathbf{f} is the body force and $\ddot{\mathbf{x}}$ is the acceleration of the body

- Mass conservation:

$$\rho V = \rho_0, \quad (7.2)$$

where ρ_0 is the reference density and $V = \det F_{ij} = \det \frac{\partial x_i}{\partial X_j}$ is the relative volume or the determinant of the deformation gradient matrix.

- Energy balance equation:

$$\dot{E} = V s_{ij} \dot{\varepsilon}_{ij} - (p + q) \dot{V} \quad (7.3)$$

where s_{ij} are the deviatoric stresses and p is the pressure, which can be calculated as follows,

$$s_{ij} = \sigma_{ij} + (p + q) \delta_{ij}, \quad (7.4)$$

$$p = -\frac{1}{3} \sigma_{ij} \delta_{ij} - q = -\frac{1}{3} \sigma_{kk} - q, \quad (7.5)$$

where q is the bulk viscosity, δ_{ij} is the Kronecker delta, and $\dot{\varepsilon}_{ij}$ is the strain rate tensor.

The solution seeked must also satisfy the following boundary conditions:

- The traction boundary conditions on boundary δb_1 :

$$\sigma_{ij}n_j = t_i(t) \quad (7.6)$$

- The displacement boundary conditions on boundary δb_2 :

$$x_i(X_a, t) = D_i(t) \quad (7.7)$$

- The contact discontinuity condition on boundary δb_3 when $x_i^+ = x_i^-$:

$$(\sigma_{ij}^+ - \sigma_{ij}^-)n_i = 0 \quad (7.8)$$

The integral addition of the equations (7.1), (7.6) and (7.8) can be written placing every term on the left hand side and integrating them over the correspondant volume and boundary surfaces, assuming that the variation δx_i is equal to zero in all conditions on δb_2 :

$$\int_v (\rho \ddot{x}_i - \sigma_{ij,j} - \rho f) \delta x_i dv + \int_{\delta b_1} (\sigma_{ij}n_j - t_i) \delta x_i ds + \int_{\delta b_3} (\sigma_{ij}^+ - \sigma_{ij}^-) n_j \delta x_i ds = 0 \quad (7.9)$$

Applying the divergence theorem, and noting that $(\sigma_{ij}\delta x_i)_{,j} - \sigma_{ij,j}\delta x_i = \sigma_{ij}\delta x_{i,j}$, this leads to the weak form of the equilibrium equation¹ which is a statement of the principle of virtual work, and that is known as $\delta\pi$:

$$\delta\pi = \int_v \rho \ddot{x}_i \delta x_i dv + \int_v \sigma_{ij} \delta x_{i,j} dv - \int_v \rho f_i \delta x_i dv - \int_{\delta b_1} t_i \delta x_i ds = 0 \quad (7.10)$$

On another note, the coordinates of the points inside the elements into which the body is divided, can be written mathematically through the following expression:

$$x_i(X_\alpha, t) = x_i(X_\alpha(\xi, \eta, \zeta), t) = \sum_{j=1}^k N_j(\xi, \eta, \zeta) x_i^j(t), \quad (7.11)$$

¹To develop the finite element equations, the partial differential equations must be restated in an integral or "weak" form. A weak form of the differential equations is equivalent to the governing equation and boundary conditions, i.e. the strong form. In many disciplines, the weak form has specific names; for example, it is called the principle of virtual work in stress analysis.[21].

where N_j are the shape functions in the parametric system of coordinates (ξ, η, ζ) , k is the number of nodal points defining the element, and x_i^j is the nodal coordinate of the j^{th} node in the i^{th} direction. Since the body is discretized into n elements, the integral in (7.10) may be separated using the spatial additivity of integration into n terms, one for each element. Then, the contribution of each element can be assembled back into a system of equations. Implementing the expression of the coordinate of the points inside the finite elements interconnected at nodal points on the isoparametric system (7.11) into this final system of equations yields the most important equation in this model:

$$\sum_{m=1}^n \left\{ \int_{v_m} \rho \mathbf{N}_m^T \mathbf{N}_m \mathbf{a} dv + \int_{v_m} \mathbf{B}_m^T \boldsymbol{\sigma} dv - \int_{v_m} \rho \mathbf{N}_m^T \mathbf{b} dv - \int_{\partial b_1} \mathbf{N}_m^T \mathbf{t} ds \right\} = 0 \quad (7.12)$$

where \mathbf{N} is the interpolation matrix, $\boldsymbol{\sigma}^T = (\sigma_{xx}, \sigma_{yy}, \sigma_{zz}, \sigma_{xy}, \sigma_{yz}, \sigma_{zx})$ is the stress vector, \mathbf{B} is the strain displacement matrix, \mathbf{a} is the nodal acceleration vector, \mathbf{b} is the body force loads and \mathbf{t} is the traction load.

7.2 Composite Layup Structure

The main element types in LS Dyna that are relevant for the present project, along with their specific nomenclature, are shown in Tab. 7.1.

Element Type	Integration technique	Description	Nomenclature
Solid	Reduced 1-point	Hexahedron, 1 integration point in the centroid	*SECTION_SOLID ELFORM=1
	Full	Hexahedron, 8 integration points	*SECTION_SOLID ELFORM=2

Table 7.1: Solid element types description and LS Dyna nomenclature.[31]

7.2.1 Solid Elements

In this part, more characteristics of the solid element with 8 nodes (hexahedron or brick element) are explained. This is one of the most reliable and robust element type in numerical analysis, particularly for impact phenomena modelling.

In Fig. 7.1 an eight node solid hexahedron element along with a table indicating the isoparametric local coordinates of its 8 nodes.

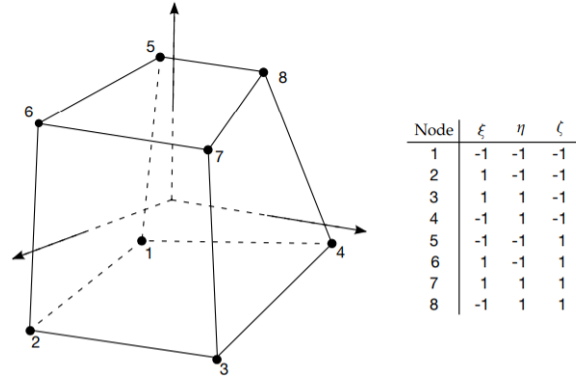


Figure 7.1: Eight node solid hexahedron element.[43]

There are some important relationships that have been introduced in the previous section 7.1 and that should be particularized for the case of a 8-node hexahedron. The coordinates of the points inside the element that construct the mesh (7.11), the shape function ϕ_j and the interpolation matrix N (3x24) for this type of elements can be expressed as follows:

$$x_i(X_\alpha, t) = x_i(X_\alpha(\xi, \eta, \zeta), t) = \sum_{j=1}^8 \phi_j(\xi, \eta, \zeta) x_i^j(t) \quad (7.13)$$

$$\phi_j = \frac{1}{8} (1 + \xi \xi_j) (1 + \eta \eta_j) (1 + \zeta \zeta_j) \quad (7.14)$$

$$N(\xi, \eta, \zeta) = \begin{bmatrix} \phi_1 & 0 & 0 & \phi_2 & 0 & \cdots & 0 & 0 \\ 0 & \phi_1 & 0 & 0 & \phi_2 & \cdots & \phi_8 & 0 \\ 0 & 0 & \phi_1 & 0 & 0 & \cdots & 0 & \phi_8 \end{bmatrix}, \quad (7.15)$$

Regarding the resolution of the system of equations of interest (7.12), one must compute the strain-displacement matrix \mathbf{B} for the solid element:

$$\mathbf{B} = \begin{bmatrix} \frac{\partial}{\partial x} & 0 & 0 \\ 0 & \frac{\partial}{\partial y} & 0 \\ 0 & 0 & \frac{\partial}{\partial z} \\ \frac{\partial}{\partial y} & \frac{\partial}{\partial x} & 0 \\ 0 & \frac{\partial}{\partial z} & \frac{\partial}{\partial y} \\ \frac{\partial}{\partial z} & 0 & \frac{\partial}{\partial x} \end{bmatrix} \mathbf{N}. \quad (7.16)$$

The terms of this matrix are readily calculated thanks to the use of the Jacobian matrix²:

$$\begin{bmatrix} \frac{\partial \phi_i}{\partial x} \\ \frac{\partial \phi_i}{\partial y} \\ \frac{\partial \phi_i}{\partial z} \end{bmatrix} = \mathbf{J}^{-1} \begin{bmatrix} \frac{\partial \phi_i}{\partial \xi} \\ \frac{\partial \phi_i}{\partial \eta} \\ \frac{\partial \phi_i}{\partial \zeta} \end{bmatrix} \quad (7.17)$$

7.2.2 Integration Method

In this part the integration process in solid elements is briefly introduced. To carry out the volume integration required for the resolution of (7.12) in a solid element, a Gaussian quadrature is introduced. This means that, being g some function defined over a volume and n is the number of integration points, the integral can be approximated by:

$$\int_v g dv = \int_{-1}^1 \int_{-1}^1 \int_{-1}^1 g |\mathbf{J}| d\xi d\eta d\zeta \approx \sum_{j=1}^n \sum_{k=1}^n \sum_{l=1}^n g(\xi_j, \eta_k, \zeta_l) |J_{jkl}| w_j w_k w_l \quad (7.18)$$

where w_j, w_k, w_l are the weighting factors, $g_{jkl} = g(\xi_j, \eta_k, \zeta_l)$ is the value of the function in the evaluation point and J is the determinant of the Jacobian matrix. The typical option employed in LS-Dyna, due to its low computational cost and to eliminate the locking issue experienced by fully integrated elements, is the one-point integration quadrature, characterized by:

$$\begin{aligned} n &= 1 \\ w_j &= w_k = w_l = 2 \\ \xi_1 &= \eta_1 = \zeta_1 = 0 \end{aligned}$$

The integration can be performed at the origin of the coordinate system $\xi = \eta = \zeta = 0$ to take advantage in the anti-symmetry property of the strain matrix at this point,

$$\begin{aligned} \frac{\partial \phi_1}{\partial x_i} &= -\frac{\partial \phi_7}{\partial x_i}, \frac{\partial \phi_3}{\partial x_i} = -\frac{\partial \phi_5}{\partial x_i}, \\ \frac{\partial \phi_2}{\partial x_i} &= -\frac{\partial \phi_8}{\partial x_i}, \frac{\partial \phi_4}{\partial x_i} = -\frac{\partial \phi_6}{\partial x_i}, \end{aligned} \quad (7.19)$$

thanks to which the effort required to compute this matrix is usually reduced.

$${}^2\mathbf{J} = \begin{bmatrix} \frac{\partial x}{\partial \xi} & \frac{\partial y}{\partial \xi} & \frac{\partial z}{\partial \xi} \\ \frac{\partial x}{\partial \eta} & \frac{\partial y}{\partial \eta} & \frac{\partial z}{\partial \eta} \\ \frac{\partial x}{\partial \zeta} & \frac{\partial y}{\partial \zeta} & \frac{\partial z}{\partial \zeta} \end{bmatrix}$$

7.3 Hourglass Control Algorithm

In Tab. 7.2 the different hourglass control algorithms available in LS Dyna are presented, along with their specific terminology. Note that the relevant options employed in the present project have been **remarked**.

Hourglass /Element	Viscous	LS Dyna	Stiffness	LS Dyna
Solid	Standard	IHQ=1	Flanagan-Belytschko	IHQ=4,5
	Flanagan-Belytschko	IHQ=2,3	More Advanced	IHQ=6,7,9
Shell	Flanagan-Belytschko	IHQ=1,2,3	Classical	IHQ=4,5,6
			Warping stiffness formulation fully integrated shells	IHQ=16

Table 7.2: Hourglass Algorithm description and LS Dyna nomenclature.

7.3.1 Viscous Hourglass Control

The resisting forces are computed based on the nodal velocity vector. The hourglass control is orthogonal to all modes, except the zero energy hourglass modes and, instead of resisting components of the bilinear velocity field that are orthogonal to the strain, the algorithm is designed to resist components of the velocity field that are not part of a fully linear field, \dot{x}_i^{kLIN} and that belong to the so-called hourglass velocity field, \dot{x}_i^{kHG} .

$$\dot{x}_i^{kHG} = \dot{x}_i^k - \dot{x}_i^{kLIN}, \quad (7.20)$$

$$\dot{x}_i^{kLIN} = \dot{\bar{x}}_i + \dot{\bar{x}}_{i,j} (x_j^k - \bar{x}_j), \quad (7.21)$$

where $\bar{x}_i = \frac{1}{8} \sum_{k=1}^8 x_i^k$ and $\dot{\bar{x}}_i = \frac{1}{8} \sum_{k=1}^8 \dot{x}_i^k$. The hourglass shape vectors computed by this algorithm, $\gamma_{\alpha k}$, can be expressed in terms of the base vectors treated previously, $\Gamma_{\alpha k}$ as:

$$\gamma_{\alpha k} = \Gamma_{\alpha k} - \phi_{k,i} \sum_{n=1}^8 x_i^n \Gamma_{\alpha n}. \quad (7.22)$$

These shape vectors are orthogonal to all the velocities embedded in the linear velocity field \dot{x}_i^{kLIN} . The product expressed previously in (7.21) is now $g_{i\alpha} = \sum_{k=1}^8 \dot{x}_i^k \gamma_{\alpha k} = 0$, and the resisting hourglass forces can be expressed as:

$$f_{i\alpha}^k = a_h g_{i\alpha} \gamma_{\alpha k}, \quad (7.23)$$

where a_h is the constant defined previously in this same section. Moreover, it should

be noted that LS Dyna includes two integration options when choosing to work with a stiffness hourglass control. For more information on this please refer to the Theory Manual [43].

7.3.2 Stiffness Hourglass Control

The stiffness hourglass control types calculates the resisting force vector proportional to total hourglass deformation. This form of hourglass control allows elements to spring back and will absorb less energy than the viscous forms. In other words, the hourglass stiffness is evaluated rather than the viscosity.

The hourglass rates are multiplied by the solution time step to produce increments of hourglass deformation. The hourglass stiffness is scaled by the element's maximum frequency so that stability can be maintained as long as the hourglass scale factor is sufficiently small.

7.4 Material formulation

In this part, some additional information on the material formulation cards defined in LS Dyna is given. This section is focused first on explaining the method define the fibre direction in a composite material. Then, more insight is provided on the specific material models employed in this present project for both developed models (high and low velocity impact on composite plates).

7.4.1 Material Direction: AOPT and parameters

The numerical parameter that defines the method to compute direction of the fibers, AOPT, is given inside the material formulation card. Inside the material card, there are other 14 parameters linked with the directional definition of its properties.

Before entering the different fibre-angle definition methods, the different coordinate systems present in LS DYNA, shown in Fig. 7.2, need to be described:

- **Global coordinate system (X-Y-Z):** Default system in LS-DYNA used for geometry, boundaries and loads.
- **Local element coordinate system:** Each element has its own coordinate system determined by the node connectivity. The stress update at the element level is performed in this local coordinate system.
- **Material coordinate system (a-b-c):** This is the coordinate system linked with the material direction-dependent properties.

- **Local user defined coordinate system:** The user can specify a local coordinate systems to be used e.g. with load options etc.

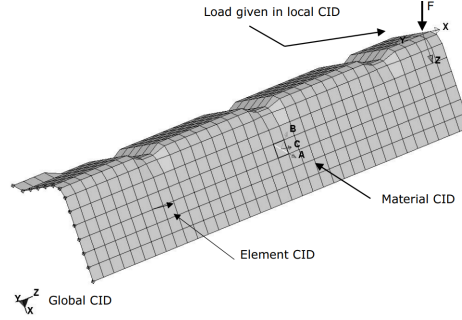


Figure 7.2: Coordinate Systems LS Dyna. [41]

There are two possible methods to specify the material coordinate system (a, b and c axis vectors) **for solid** elements in LS DYNA.

1. Inside the material formulation through the **AOPT option**. This method is able to compute the material coordinate system directions by defining different input values. There are particularly two methods of interest for this work:

- **Global orthotropic (AOPT=2):** The material system is based on global entities, a vector a coincident with the material principal direction, and other vector d . This is the one employed for both constructed models in this present work.

$$\mathbf{c} = \mathbf{a} \times \mathbf{d} \quad (7.24)$$

$$\mathbf{b} = \mathbf{c} \times \mathbf{a} \quad (7.25)$$

Easier but also not recommendable for complex geometries.

- **Local orthotropic (AOPT=3):** The material system definition is based on local entities, a vector v and an angle β .

$$\mathbf{a} = \mathbf{v} \times \mathbf{n} \quad (7.26)$$

$$\mathbf{b} = \mathbf{n} \times \mathbf{a} \quad (7.27)$$

where \mathbf{n} is the normal of a midsurface determined by node connectivity. Once the vectors \mathbf{a} and \mathbf{b} are computed they are rotated counterclockwise by β . This option is recommended in complex geometry cases as it is completely based in local values.

2. Rotating the initially defined material coordinate system in AOPT by an angle specified in the element formulation.

- Setting a rotation angle inside the element formulation (*ELEMENT_SOLID_ORTHO). The system a-b-c defined inside the material formulation is rotated by an angle specified in the card (A1).

Another relevant parameter related with the definition of the fiber direction is the one known as **Invariant Node Numbering (INN)**. This option must be activated to make direction dependent materials independent of a change in element connectivity (local coordinate system). For **solids**, this option defines vectors from the center of one face to the opposite face. Then, cross products are made from these vectors and dot products are made between the cross products. Then, the vectors and testing are done to make an orthogonal system. This is computationally more expensive than for shells.

For both models in this work, due to the simplicity of the geometry the option chosen to define **material coordinate system is based on global entities, AOPT=2**. The necessary input values for this option are, the vector a , which defines the fiber axial direction (principal direction of the material), and another auxiliar vector d , which in this case coincides with the perpendicular direction to fibers. The third direction is computed easily as $c = a \times d$.

7.4.2 Material Formulations Specifications

This section is focused on specifying what are the parameters involved in the definition of the composite material formulation cards used for the developed models. The main formulations employed were the enhanced composite damage material (054/055) and the elastic orthotropic composite (002), which was used for the low velocity sub-model focused on delamination.

Material model 54: Enhanced Composite Damage

The composite plate is defined in both models, high and low velocity impacts, with the enhanced composite damage material formulation (*MAT_054 or *MAT_ENHANCED_COMPOSITE_DAMAGE). A detailed description on the parameters involved in this formulation was given in section 3.3.3. However, the whole material card and a brief description on the strength softening parameters, which were not included in the present developed models, are given here.

The full material card is presented in Fig. 7.3

*MAT_ENHANCED_COMPOSITE_DAMAGE_(TITLE) (054/055) (4)

TITLE									
T800S/M21 -45deg									
1	MID	RO	EA	EB	(EC)	PRBA	(PRCA)	(PRCB)	
	101	1.550e-09	1.650e+05	7640.0000	7640.0000	0.0162000	0.0162000	0.4000000	
2	GAB	GBC	GCA	KF	AOPT	2WAY			
	5610.0000	2750.0000	5610.0000	0.0	2.0000000	0.0			
3	XP	YP	ZP	A1	A2	A3	MANGLE		
	0.0	0.0	0.0	-0.7071000	0.7071000	0.0	0.0		
4	V1	V2	V3	D1	D2	D3	DFAILM	DFAILS	
	0.0	0.0	0.0	-0.7071000	-0.7071000	0.0	0.0366000	0.0	
5	TFAIL	ALPH	SOFT	FBRT	YCFAC	DFAILT	DFAILC	EFFS	
	0.0	0.0	1.0000000	0.0	2.0000000	0.0133000	-0.0072700	0.0	
6	XC	XT	YC	YT	SC	CRIT	BETA		
	1200.0000	2200.0000	280.00000	45.000000	50.000000	54.0	1.0000000		
7	PEL	EPSE	EPSR	TSMD	SOFT2				
	0.0	0.0	0.0	0.0	1.0000000				
8	SLIMT1	SLIMC1	SLIMT2	SLIMC2	SLIMS	NCYRED	SOFTG		
	0.0	0.0	0.0	0.0	0.0	0.0	1.0000000		
9	LCXC	LCXT	LCYC	LCYT	LCSC	DT			
	0	0	0	0	0	0.0			

Damage factors →

Constitutive

Fiber orientation

Erosion strains to failure

Damage Onset (Material Strengths)

Figure 7.3: Material formulation 54 model card in LS Dyna (Enhanced Composite Damage). [44]

Inside this material card, multiple numerical parameters are in charge of degrading the fiber strengths when matrix failure takes place. These are:

- **FBRT**: Reduction factor for tensile fiber strength after matrix failure.

$$X_t^* = X_t \cdot FBRT \quad (7.28)$$

- **YCFAC**: Reduction factor for tensile fiber strength after matrix failure.

$$Y_t^* = Y_t \cdot FBRT \quad (7.29)$$

- **SOFT**: Strength reduction factor for crush simulations of the elements immediately ahead of the crush front to simulate damage propagating from the crush front.

$$\{XT, XC, YT, YC\} = \{XT, XC, YT, YC\}^* \cdot SOFT \quad (7.30)$$

The SOFT parameter is defined between [0-1] and since it cannot be measured experimentally, it must be calibrated by trial and error for crush simulations.

Note that, these parameters are very difficult to measure through experimental tests and, thus, should be estimated by trial and error [20].

7.4.3 Material model 002: Orthotropic Elastic material

This constitutive law is simpler than the previous one as it only models the elastic behaviour of the composite. This is why a lower number of parameters is needed to define this material model. The material card is shown in Fig. 7.4.

*MAT_ORTHOTROPIC_ELASTIC_(TITLE) (002) (4)

TITLE							
T800S/M21 -45deg elastic							
1	MID	RO	EA	EB	EC	PRBA	PRCA
	101	1.550e-06	165.00000	7.6399999	7.6399999	0.0162000	0.0162000
2	GAB	GBC	GCA	AOPT	G	SIGF	
	5.6100001	2.7500000	5.6100001	2.0	0.0	0.0	
3	XP	YP	ZP	A1	A2	A3	MACF
	0.0	0.0	0.0	-0.7071000	0.7071000	0.0	1
4	V1	V2	V3	D1	D2	D3	BETA
	0.0	0.0	0.0	-0.7071000	-0.7071000	0.0	0.0
							REF
							0.0

Constitutive

Fiber orientation

Figure 7.4: Material formulation 2 model card in LS Dyna (Elastic Orthotropic material law.)

The difference in the constitutive law of the composite modelled with these two formulations, are presented in Fig. 7.5, where the fibre stress-strain curves are presented for the correspondant uniaxial fibre-direction tension tests.

Note that the formulations of interest for this project are represented as: the elastic orthotropic law (*MAT_002, red curve) and the enhanced composite damage option (*MAT_054, dark blue curve) along with other LS Dyna formulations.

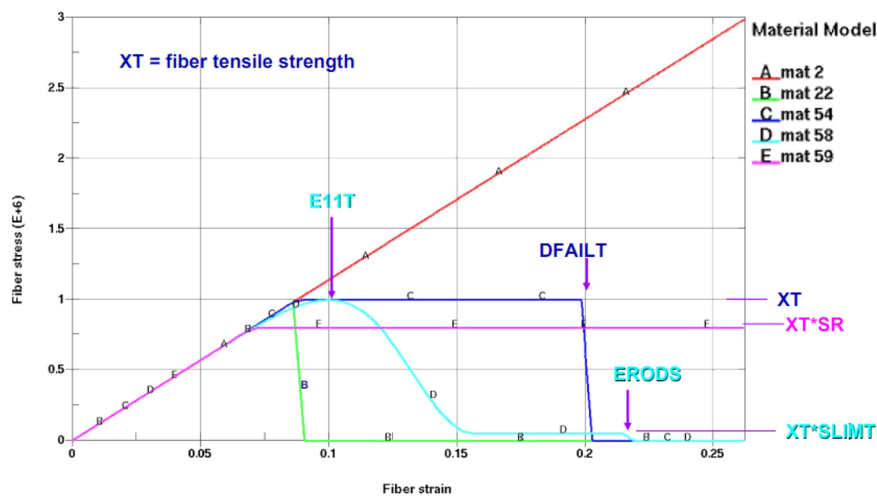


Figure 7.5: Stress-strain curves in uniaxial tension test in the fiber direction, for different composite material constitutive laws available in LS Dyna.[34]

7.5 Contact Algorithm

In this section we give some additional information on the contact modelling techniques available in LS Dyna. The classification of the multiple contact formulations, a detailed explanation on the contact search method, and on the penalty-based contact parameters, are given as complementary information for the section dedicated to the construction of the contact algorithm. In addition, some extra specifications for the contact models in this project are given in order to provide enough information to the reader to reproduce this model entirely on his own.

7.5.1 Classification of contacts

There are two primary ways to distinguish contact algorithms, the **method used to search for penetration** and the method of **applying contact forces** after such penetration is found.

Contact search methods are classified between the **node-based search** (non-automatic formulation), the **bucket sort** approach (automatic formulation), and the **segment-based search**. These three methods are further explained in the first part of this section.

As for the contact force calculation methods, there are two relevant methodologies implemented in LS-Dyna:

- **Constraint-based:** Based on a kinematic constraint between nodes of one part and segments of the other. Constraints are imposed on the global equations by a transformation of the nodal displacement components of the slave nodes along the contact interface, which consists in eliminating the normal degree of freedom of the slave nodes.
- **Penalty-based:** The method consists of placing normal interface artificial springs between the penetrating nodes and the contact surface master segments. There are three possible ways of implementing the contact algorithm:
 - **Standard Penalty Formulation (SOFT=0):** Detects penetration of nodes into segments and applies penalty forces to the penetrating node and the segment nodes. The penalty stiffness is calculated based on the material properties.
 - **Soft Constraint Penalty Formulation (SOFT=1):** Option implemented to treat contact between bodies with dissimilar material properties (e.g. steel-foam), as the penalty stiffness and its update during the simulation is not based on the material.
 - **Segment-based Penalty Formulation (SOFT=2):** Detects penetration of one segment into another segment and then applies penalty forces to nodes of

both segments. The calculation of the penalty stiffness is similar to the Soft Constraint formulation.

7.5.2 Contact Search

In LS-DYNA, a contact is defined by identifying what locations are to be checked for potential penetration of a slave entity (node or segment) through a master segment. A search for penetrations, using any of a number of different algorithms is made every time step. The penetration search methods can be classified between:

- **‘Old’ Node-based:** Non-automatic contacts search for penetration. This algorithm finds for each slave node its nearest point on the master surface (perpendicular direction). This method is not good for disjoint or irregular meshes and requires of correct orientation of segments.
- **Bucket Sort Approach:** This approach is the most commonly used by automatic contacts (always preferred over non-automatic contacts), as it is more adequate for non-continuous surfaces. The idea is to locate the nearest segment to the slave node. The idea behind a bucket sort is to perform some grouping of the nodes, so that the sort operation needs only to calculate the distance of the nodes in the nearest groups. In a direct search of N nodes, to search for the nearest node the total number of distance comparisons is $N \cdot (N - 1)$. In bucket search, we consider a partitioning of the surface as the one shown in Fig. 7.6. With this partitioning the nearest node will, either reside in the same bucket, or in one of the two adjoining buckets, so the total number of distance operations is reduced to,

$$N \cdot \left(\frac{3N}{a} - 1 \right) \text{ for 1D cases,} \quad (7.31)$$

$$N \left(\frac{9N}{ab} - 1 \right) \text{ for 2D cases,} \quad (7.32)$$

$$N \left(\frac{27N}{abc} - 1 \right) \text{ for 3D cases,} \quad (7.33)$$

where a , b and c are the number of partitions along the partitioning dimensions. It should be also noted that for this search technique, the orientation of the segments is not important, which means that contact is searched from both sides of a shell, as opposed to the based node-search.

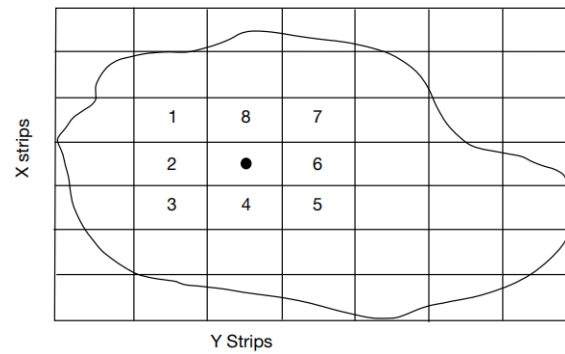


Figure 7.6: 1D and 2D bucket sorting. [43]

- **Segment-based:** Searches for penetration between segments. In other words, a segment A is deemed to have penetrated another segment B when at least one node of segment A has penetrated each of the five planes associated with segment B. It should be noted that it is not necessary that the same node of segment A penetrates each of the five planes, which consist of the plane containing the segment plus the four edge planes³ of the segment [43]. Segment-based contact is a good option if contact surface is not smooth, perhaps having sharp corners or edges.

Concerning the search method employed, the contact options can also be divided between one or two way contacts. In the one-way option, only the slave nodes are checked for penetration. While in the two-way contacts, the masters and slaves are reversed and contact checked both ways. Typically, if the name of the contact does not specify it, the contact is two-way.

7.5.3 Penalty-based Contact

The physics behind the penalty contact problem are explained in this section. Considering the following system:

³An edge plane is defined as being perpendicular to the segment and containing one edge of the segment.

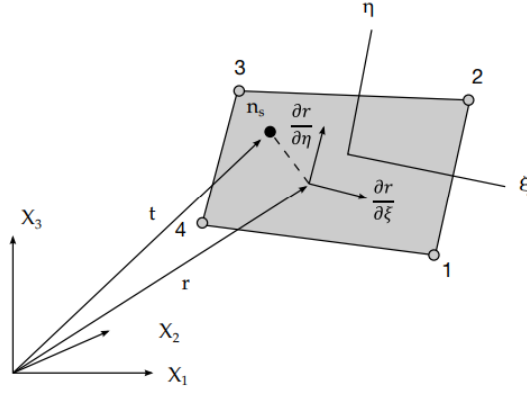


Figure 7.7: Location of contact point when slave node lies above master segment. [43]

The penalty problem starts with a slave node n_s penetrating its corresponding master segment which has a thickness offset value t . The penetration is detected and its depth l is calculated,

$$l = \mathbf{n}_i \times [\mathbf{t} - \mathbf{r}(\xi_c, \eta_c)] < 0 \quad (7.34)$$

To counteract this penetration, an interface force, \mathbf{f}_s , is applied to the degrees of freedom corresponding to the slave node (n_s),

$$\mathbf{f}_s = -l \cdot k_i \cdot \mathbf{n}_i \text{ if } l < 0. \quad (7.35)$$

The slave node is projected back up to the surface of the master segment. Finally, a reaction force f_m^i , is applied to the master segment nodes, such that the total force on the master nodes equals the applied slave node force. Note that, n_i is the unit normal to the master segment at the contact point, k_i is the stiffness of the numerical (artificial) contact spring and l the penetration depth.

In Fig. 7.8, a more visual description of the penalty method and its parameters is shown.

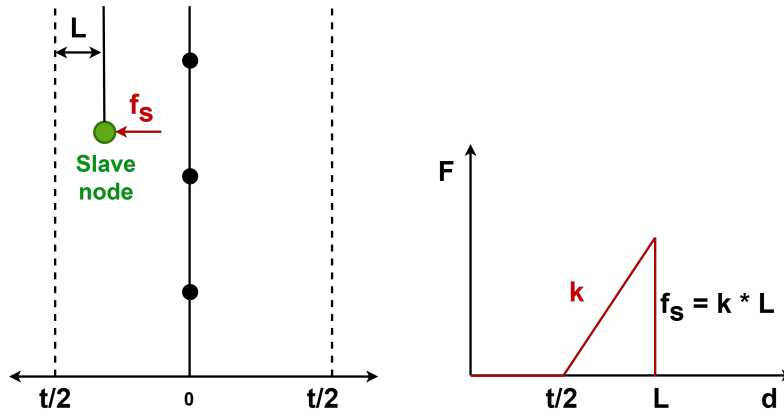


Figure 7.8: Penalty Based Theory of Contact.

Note that, the left graph represents the slave node (green dot) penetration through the master segment (dotted line). The penetration is detected when the slave node surpasses the contact thickness, t , assigned to the master segment. Once the penetration is detected, the penalty forces, f_s are applied to the slave node. The right plot, presents the evolution of the penalty force applied through the artificial "contact spring" as a function of the distance, d , coordinate.

As it was already explained, the penalty-based contact is based on different parameters. The **contact thickness** (t) which determines the thickness offsets in contact and that can be classified in:

- **Shell thickness:** Specified in the specifications of the shell element. This thickness affects the mass and stiffness of the element.
- **Contact thickness:** The default value is normally, either the shell thickness or 40% of the element edge. This value is set in the specifications of the contact algorithm and does not affect the stiffness or mass of the shell but the maximum penetration depth allowed for the contact before the slave nodes are set free.

The second parameter is the **penalty stiffness** (k_i) of the artificial springs introduced to simulate the penalty contact. This value can be computed through different methodologies:

1. **Default penalty formulation (SOFT=0)**, suited for contact between similar stiff materials. The stiffness is calculated as follows:

$$k_i = \frac{f_{si} K_i A_i^2}{V_i} \text{ for solid elements} \quad (7.36)$$

$$k_i = \frac{f_{si} K_i A_i}{\max(\text{shell diagonal})} \text{ for shell elements} \quad (7.37)$$

where, f_{si} is the penalty factor (SFS and SFM in LS Dyna), A_i refers to the area of the contact segment, K_i is the bulk modulus of the material established for the contacted element $K = \frac{E}{1-2\nu}$. In LS-DYNA, a number of options are available for setting the penalty stiffness value. This is often an issue since the materials in contact may have drastically different bulk moduli. The default option that LS Dyna selects for the the stiffness is the minimum between the master segment and the slave node. However, there are other possibilities (PENOPT) and it should be noted that for a contact between shell and a solid element segments, the shell determines the stiffness always.

2. **Soft Constraint Penalty (SOFT=1)**, better suited for soft materials. The contact between soft and stiff materials results in an undesired effect on the contact stiffness, lowering its value and ultimately causing excessive penetration. By choosing this

option, an additional stiffness is calculated. This stiffness is based on the Courant's criterion or in the stability of the local system, comprised of two masses (segments) connected by a spring:

$$k_{cs}(t) = 0.5 \cdot \text{SOFSCCL} \cdot m^* \cdot \left(\frac{1}{\Delta t_c(t)} \right)^2, \quad (7.38)$$

where SOFSCCL is the scale factor, m^* is a function of the mass of the slave node and of the master nodes, δt is set to the initial solution timestep. If the solution time step grows, δt_c is reset to the current time step to prevent unstable behavior. This type of contact is normally used for contact between parts with dissimilar material properties, or dissimilar mesh densities, like the one studied in this work. A comparative check against the contact stiffness calculated with the traditional penalty formulation is done, and the maximum value is chosen.

3. **Segment-Based Penalty formulation (SOFT=2)**, well-suited for dissimilar material interactions like the previous option, but in this case with a segment to segment search approach. As for the penalty stiffness calculation method, it is similar to SOFT=1. The penalty force is applied to both segments involved in the contact:

$$k_{cs}(t) = 0.5 \cdot \text{SLSFAC} \cdot \left\{ \begin{array}{c} \text{SFS} \\ \text{or} \\ \text{SFM} \end{array} \right\} \left(\frac{m_1 m_2}{m_1 + m_2} \right) \left(\frac{1}{\Delta t_c(t)} \right)^2 \quad (7.39)$$

In this case, segment masses (m_1 and m_2)⁴ are used rather than nodal masses.

Another special feature of this option is that initial penetrations are ignored by default without the need of any additional parameters. That is, there is no perturbation of the geometry to alleviate initial penetrations. However, the penetrations are not completely deleted from the problem, but for each segment pair they are stored and subtracted from the current penetration before calculating penalty forces. The purpose of this logic is that a segment that penetrates undetected for a brief period is not shot out by a large penalty force once detected.

Finally, two of the specific field parameters of this option should be mentioned. First, SBOPT which is in charge of determining the penetration check methodology. The recommended SBOPT is always the warped segment option (SBOPT=3), as it accurately checks for penetration of warped surfaces. The second parameter is related to the search depth for nodal penetrations through the closest contact

⁴The segment mass is equal to the element mass for shell segments and half the element mass for solid element segments.

segments, DEPTH. The recommended value is DEPTH=5 when using SOFT=2, as both surface penetrations and edge-to-edge penetrations are checked.

7.5.4 Contacts Additional Specifications

Projectile-Plies Contact

The contact formulation for this interaction in both models (high and low velocity impact) was *CONTACT_AUTOMATIC_ERODING _SURFACE_TO_SURFACE. Some more additional specifications of this contact are included in this section.

The _AUTOMATIC keyword indicates that a two-way contact formulation is employed, which means that the master and slave distinction is not important.

The _ERODING keyword allows the contact surface to be updated as elements on the free surface are deleted due to material failure criteria. As slave nodes become unattached/free due to element deletion, those nodes may optionally continue to be considered in the contact or removed from the problem by the parameter ENMASS. The eroding contact used in this case is the *CONTACT_ERODING _SURFACE_TO_SURFACE, in which the slave and the master sides are defined through parts or part sets. There are also other possibilities:

- ***...NODES_TO_SURFACE:** The slave side of the contact is a node set containing all the nodes of the slave side part(s). A bucket sort is performed after each time step in which an element is deleted. This type is recommended for bird-to-blade contact in bird strike simulations.
- ***...SINGLE_SURFACE:** It is based on the single surface contact algorithm, which includes all the contact sides as slave parts. This option does not only allows for erosion representation in the projectile-plies contact interface, but also on all the contact interfaces between plies and in the plies self-contact. This model is way too complex to introduce this contact option, since it introduces much larger computational efforts and instabilities in the contact calculations.

Interply Contact

This contact interaction employs the *CONTACT_AUTOMATIC_SINGLE _SURFACE LS Dyna option, and is introduced whenever the eroding contact explained previously is also used in the models. This contact is defined between all the plies of the plate, which are all part of the slave side, and is active when ply elements get deleted and non-subsequent plies come into contact, or when there is compressive buckling (self-contact) present in the plies.

The most relevant characteristic is that, since the contact occurs between plies with similar materials and mesh sizes, the penalty stiffness is calculated with the default formulation $\text{SOFT}=0$, unlike in the previous case.

Delamination Contact

The third contact interaction defined in both models actually aims to represent, not only the contact between subsequent plies, but also the possible delamination between different fibre-oriented plies. For this purpose the LS Dyna formulation `*CONTACT_TIEBREAK_SURFACE_TO_SURFACE` is used. This contact is already explained in detail in the manuscript, so only a few additional notes are made on the tying conditions and on the theoretical basis of the $\text{OPTION}=9$'s tiebreak delamination method.

First, the **criteria for tying a slave node to a master segment** should be described. Note that, if the criteria are not met, the node is not tied and a warning is issued during the simulation. It is highly recommended to specify only the nodes or segments you want to be considered for tying (node sets or segment sets rather than parts or part sets). With this tip, undetection of tied conditions can be avoided. The tying conditions in tiebreak contacts are:

1. The slave node lies within the orthogonal projection of a master segment.
2. The gap between the slave node and its master segment is less than a specific value based on element dimensions. The tolerance can usually be overridden, e.g., by specifying a negative contact thickness.

$$D < 0.6 * (\text{master thickness} + \text{slave thickness}) \quad (7.40)$$

Inside the tiebreak contact model, there are different options to model delamination. The choice of which option to use depends on the requirements of the model and of the allowable parameters, which requires for standard ATSM material tests to be carried out.

These options can be classified depending on the damage law employed to model the evolution of delamination through the composite plate. This was already explained in detail in section 3.3.4, where it was clearly indicated that **OPTION=7** is the simplest approach without any damage model, **OPTION=6** is intermediate as it uses a linear law for delamination growth, and finally, **OPTION=9** is the most complex case with a bilinear damage law with possibility of representing a mixed-mode loading condition.

In this section, the objective is to provide a more detailed explanation of the most complex delamination modelling option ($\text{OPTION}=9$) used in this work. This option is similar to using cohesive elements, which features a bilinear traction-separation law, mixed

mode delamination, and peak tractions as function of element size. The two modes of delamination described are opening (I), shear (II) and a third mode known as tear (III) which is going to be inside the second mode. The peak tractions (S,T), which note the onset of damage for each mode, can be defined as functions of characteristic element length (square root of master segment area) using load curves. With these options, nearly the same global responses (for instance, load-displacement curve) can be obtained with coarse meshes compared to fine meshes. The only limitation of choosing this method to model delamination is the need of the adequate the material parameters.

The model is graphically represented in Fig. 7.9

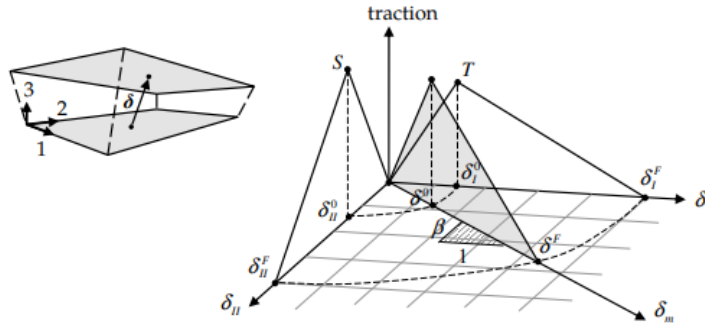


Figure 7.9: Mixed-mode traction separation law. [32]

For the individual modes I and II, the onset of delamination takes place at the following values of the relative displacements:

$$\delta_{I0} = \frac{\sigma_n}{k_I} \quad (7.41)$$

$$\delta_{II0} = \frac{\sigma_s}{k_{II}} \quad (7.42)$$

Correspondingly the failure or ultimate relative displacements occur when,

$$\delta_{Im} = \frac{2\mathcal{G}_{Ic}}{k_I \delta_{I0}} \quad (7.43)$$

$$\delta_{II_m} = \frac{2\mathcal{G}_{IIc}}{k_{II} \delta_{II0}} \quad (7.44)$$

For the mixed mode, the relative displacement can be approximated by a quadratic interaction between the two modes,

$$\delta = \sqrt{\langle \delta_I \rangle^2 + \delta_{II}^2}, \quad (7.45)$$

where, δ_{II} accounts for both the shear and the tear fracture modes, $\delta_{II} = \sqrt{\delta_{\text{shear}}^2 + \delta_{\text{tear}}^2}$.

Besides, the delamination onset relative displacement this mixed mode crack opening

condition can be expressed as follows,

$$\delta_0 = \delta_{I_0} \delta_{II_0} \sqrt{\frac{1 + \beta^2}{(\delta_{II_0})^2 + (\beta \delta_{I_0})^2}} \quad (7.46)$$

where β is a variable that represents the mode mixity and it is calculated $\beta = \max\left(0, \frac{\delta_{II}}{\delta_I}\right)$.

On the evolution of delamination, the following power law is employed,

$$\left(\frac{\mathcal{G}_I}{\mathcal{G}_{Ic}}\right)^\alpha + \left(\frac{\mathcal{G}_{II}}{\mathcal{G}_{IIc}}\right)^\alpha = 1 \quad (7.47)$$

If this power law is translated in terms of the relative displacements following the equations (7.46), the evolution of this phenomenon can be described as

$$\delta_m = \begin{cases} \frac{1 + \beta^2}{\delta_0} \left[\left(\frac{k_I}{\mathcal{G}_{Ic}}\right)^\alpha + \left(\frac{k_{II}\beta^2}{\mathcal{G}_{IIc}}\right)^\alpha \right]^{-\frac{1}{\alpha}} & \Longleftarrow \delta_I > 0 \\ \delta_{II_m} & \Longleftarrow \delta_I \leq 0 \end{cases} \quad (7.48)$$

To finalize the description of this model, one should note that the damage law can then be represented in terms of relative displacements as:

$$d = \frac{\delta_m (\delta - \delta_0)}{\delta (\delta_m - \delta_0)} \quad (7.49)$$

A final note is given on the common values employed for the damage evolution parameter α . Normally, for carbon-fibre epoxy composites one can represent the mixed mode data using $1 \leq \alpha \leq 2$.

For a better understanding, Tab. 7.3 includes the description of every parameter and its correspondance between a cohesive element and a tiebreak contact formulation in LS Dyna.

Model Parameters	Cohesive element (*MAT_138)	Tiebreak contact (OPTION=9)
Normal peak traction (T or σ_n) [MPa]	T	NFLS
Shear peak traction (S or σ_s) [MPa]	S	SFLS
Exponent mixed mode criteria (α)	XMU	PARAM
Energy release rate for mode I (G_{IC}) [$MPa \cdot mm$]	GIC	ERATEN
Energy release rate for mode II (G_{IIC}) [$MPa \cdot mm$]	GIIC	ERATES
Ratio between the normal and in-plane stiffness ($\frac{k_I}{k_{II}}$)	ET/EN	CT2CN
Stiffness normal to cohesive element mid plane (k_I) [MPa/mm]	EN	CN
Ultimate displacements ($\sigma_{Im}, \sigma_{IIIm}$) [mm]	UND, UTD	n/a

Table 7.3: Cohesive element and tiebreak contact option 9 parameters. Bilinear traction separation mixed mode law.

Chapter 8

Appendix B: Material Properties

This Appendix collects the material properties of the composite plates of the high and low velocity impact models. Besides, the material testing procedures carried out in previous studies to characterize the behaviour of the composite materials of interest are explained. These experimental data has been borrowed as an input for the present models.

8.1 High Velocity Model

The material parameters were obtained from two studies linked with the reference numerical model [6] and ballistic impact tests [39] employed as a basis in the construction of the present high velocity model.

The first resource was carried out by Kay et.al in [27], and is a characterization procedure of BMS8-212 during penetration. The second study focuses on the delamination modelling of BMS8-212, conducted by Powell et.al in [49].

8.1.1 Composite Plate: BMS8-212

BMS8-212: Ply characterization

The mechanical properties of BMS8-212 composite are shown in Tab. 8.1. Note that a denotes the fiber direction, X is the fiber direction strength, b is the transverse direction (Y is the transverse strength) and c is the normal direction (Z is the normal direction strength). The fiber direction strengths were assumed to be rate insensitive.

These properties come from the study carried out by Kay et al. [27] where they performed the characterization during penetration of a BMS8-212 composite panel. The elastic properties and fiber direction strengths were provided by Boeing, the main supplier of this fibre reinforced composite panels for aerospace applications, and from communications with Steve DeTeresa. The matrix dominated compressive strengths were measured at

LLNL, and the tensile matrix properties were estimated.

Mechanical Properties BMS 8-212	ρ (kg/m^3)	E_a (GPa)	E_b (GPa)	E_c (GPa)	ν_{ab}	ν_{ca}	ν_{cb}	G_{ab} (GPa)	G_{bc} (GPa)
	1548	117.9	8.825	8.825	0.025	0.025	0.3	5.51	2.53
Failure Parameters	X_T (GPa)	X_C (GPa)	Y_T (GPa)	Y_C (GPa)	S_C (GPa)	ϵ_T	ϵ_C	ϵ_M	ϵ_S
	1.103	1.034	0.055	0.25	0.07	9.35e-3	-8.77e-3	0.028	0.03

Table 8.1: Mechanical properties and failure parameters for material model, BMS8-212 carbon fiber-epoxy composite. [27]

BMS8-212: Delamination characterization

To determine the interlaminar toughness parameters for the high velocity model, the study developed by Powell et al. [49] was used as a reference.

This work was carried out to aid the computational modelling of airplane fragment-shielding systems. By conducting the necessary material tests, the mode I interlaminar fracture toughness of unidirectional composite samples of BMS 8-212 was determined. In the experiments presented in this study, tests were performed on five 26-ply coupons with nominal thickness of 5 mm, designed to permit fracture toughness determination according to ASTM Standard D5528-01 [3].

On another note, this study included too few tests at each loading rate to determine whether there is any rate sensitivity for the fracture toughness. In the end, it was assumed that strain rate does not have an effect on the opening energy release rate.

Loading was applied using a screw driven machine and measurements were taken on the force and crack-opening displacement. These data was then used to calculate the fracture toughness of the composites using the three methods provided in ASTM Standard D5528-01 [3]:

- **Modified Beam Theory (MBT):** This method treats the composite sample as a double cantilever beam, with each beam originating at the origin of the crack, leading to the expression for fracture toughness:

$$G_{Ic}^B = \frac{3P\delta}{2ba}. \quad (8.1)$$

However, a correction to the original model is implemented to prevent the overestimation of G_{Ic} . This correction consists in considering the crack length slightly longer than the observed length a , so the crack length is modified by $a + \Delta$, and the

corrected expression for the energy release rate is:

$$G_{Ic}^{MBT} = \frac{3P\delta}{2b(a + |\Delta|)} \quad (8.2)$$

It should be noted that, Δ is calculated from experimental data under the assumption that the beam compliance $C = \delta/P$ varies as the cube of the crack length.

- **Compliance Calibration (CC):** The fracture toughness using this method is computed as:

$$G_{Ic}^{CC} = \frac{nP\delta}{2ba} \quad (8.3)$$

where the power n , is the slope of the least-squares best fit line to a log-log a plot of the compliance (C) against the crack length (a). This method is based on the power law dependence between the compliance and the crack length as:

$$C = \alpha a^n. \quad (8.4)$$

- **Modified Compliance Calibration (MCC):** This method eliminates the use of the crack length a in the direct calculation of the fracture toughness through an identification of a parameter named A_1 similar to α , which appeared on the previous method. The fracture toughness using this method is then,

$$G_{Ic}^{MCC} = \frac{3P^2C^{2/3}}{2A_1bh}. \quad (8.5)$$

where h is the thickness of the specimen. Specifically, the MCC method identifies the parameter appearing in the expression:

$$\frac{a}{h} = A_1C^{1/3}. \quad (8.6)$$

The results shown in the study [49] proof consistency on fracture toughness calculation between the three techniques throughout the test. This agreement between methods is similar to that reported in ASTM Standard D5528-01 [3].

Finally, and considering the values at crack lengths of $\delta = 58mm$ and beyond, after determining the resistance curves (R-curves) of the five delamination coupons, the average steady-state fracture toughness is considered to be $G_{Ic} = 135J/m^2$. This is the final value that was used in the high velocity model.

The rest of the properties tiebreak contact are shown in Tab. 8.2.

Tiebreak Parameters	Description	Value
NFLS	Normal stress (σ_n) [MPa]	1357
SFLS	Shear stress (σ_n) [MPa]	10590
PARAM	Friction angle (ϕ) [rad]	0
ERATEN	Mode I fracture toughness (G_{IC}) [J/m^2]	135
ERATES	Mode II fracture toughness (G_{IIC}) [J/m^2]	400

Table 8.2: Tiebreak contact parameters implemented in high velocity impact on composite plate. [6, 39, 49]

8.1.2 Elasto-Plastic Projectile: Steel

The mechanical properties of the steel projectile are shown in Tab. 8.3.

Mechanical Properties Steel	ρ (kg/m^3)	E (GPa)	ν
	7857	206.7	0.3

Table 8.3: Mechanical properties steel impactor high velocity impact model. [39]

8.2 Low Velocity Model

8.2.1 Composite Plate: T800/M21

The mechanical properties of the T800S/M21 composite material used for the plate of the low velocity impact model are shown in Tab. 8.4.

Mechanical Properties T800S/M21	ρ (kg/m^3)	E_a (GPa)	E_b (GPa)	E_c (GPa)	ν_{ab}	ν_{ca}	ν_{bc}	G_{ab} (GPa)	G_{bc} (GPa)
	1550	157	8.5	8.5	0.35	0.35	0.53	4.2	2.2
Failure Parameters	X_T (GPa)	X_C (GPa)	Y_T (GPa)	Y_C (GPa)	S_C				
	2.2	1.2	0.045	0.28	0.045				

Table 8.4: Mechanical properties of composite failure model for T800S/M21. [25]

T800/M21: Ply Characterization

The material for the low velocity impact model was characterized thanks to the experimental tests carried out in the reference study [25], which served as the basis for the construction of this model. The material model in this work was calibrated using the results of these experiments.

The material characterization tests are presented in this section. Basically, quasi-static (tensile tests) and dynamic (Split Hopkinson's Pressure Bars, SHPB) tests were conducted to obtain mechanical properties of unidirectional composite material T800S/M21.

First, the **quasi-static tensile and shear tensile tests** in the different fibre directions were performed to the T800/M21 specimen. The results from the reference study [25] were borrowed to obtain the characteristics for the strain to failure parameters. The results of the tensile tests conducted in the samples of T800/M21 with stacking sequences $[0 \text{ deg}]_4$ and $[90 \text{ deg}]_8$ are shown in Fig. 8.1.

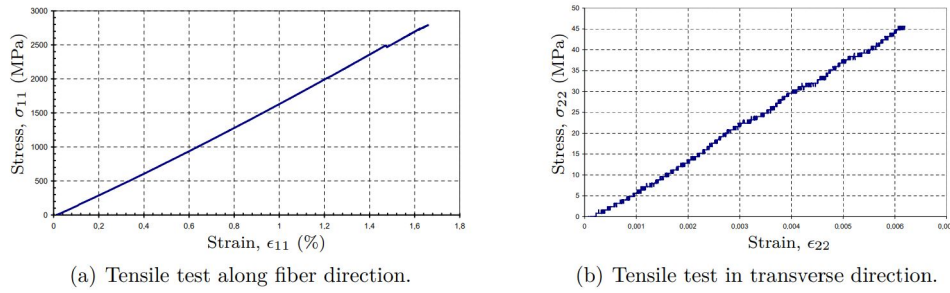


Figure 8.1: Tensile testing of T800S/M21 on samples $[0 \text{ deg}]_4$ and $[90 \text{ deg}]_8$. [25]

The results of the shear tensile tests performed on the sample with $[\pm 45]_{2s}$ are shown in Fig. 8.2:

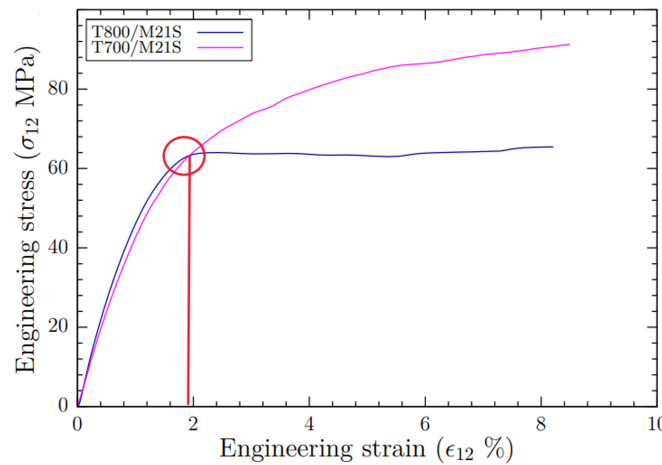


Figure 8.2: Shear tensile testing of T800S/M21 $[\pm 45]_{2s}$. [25]

The final results from the tensile tests performed on the laminates were:

- **Tensile testing** $[0]_4$: Failure stress $\sigma_{11}^r = 2698$ MPa and failure strain $\epsilon_{11}^r = 1.557\%$.
- **Tensile testing** $[90]_8$: Failure stress $\sigma_{22}^r = 48$ MPa and failure strain $\epsilon_{22}^r = 0.6\%$.
- **Shear tensile testing** $[\pm 45]_{2s}$: Failure stress $\sigma_{12}^r = 64$ MPa and failure strain $\epsilon_{12}^r = 2\%$.

Secondly, the **dynamic compression tests** or SHPB were performed in different samples to characterize the strain rate effect on the mechanical behavior of T800S/M21 samples. The strain rate effect is not a part of the present study so, the experimental tests have been only employed to obtain the failure stresses and strains as in the quasi-static case, for the compressive loading mode.

In this case, the stress-to-strain curves are not shown, since they provide much more information than the one that was actually needed, but all the results can be checked in the reference study [25].

The experimental tests employed for the calibration of the strain to failure parameters of T800/M21 were:

- **Compression of specimen** $[0]_{16}$: At a strain rate range $\dot{\epsilon} = 234 - 855s^{-1}$, failure stress vary between $\sigma_{11}^c = 960 - 1080$ MPa the failure strains $\epsilon_{11}^c = 0.0105 - 0.015$.

The compressive failure of carbon fiber plies is usually attributed to micro-buckling of fibers. This may explain the reduction in modulus and increase in failure strain, as the failure is no more pure compression of fibers but a mixed mode failure of fibers and matrix.

- **Compression of specimen** $[90]_{16}$: At a strain rate range $\dot{\epsilon} = 250 - 730s^{-1}$, the failure stress varies between $\sigma_{22}^c = 290 - 390$ MPa and the failure strain $\epsilon_{22}^c = 0.033 - 0.036$.
- **Compression of specimen** $\pm[45]_{3s}$: At a strain rate range $\dot{\epsilon} = 420 - 1100s^{-1}$, failure stress varies between $\sigma_x^c = 190 - 295$ MPa and failure strain $\epsilon_x^c = 0.07 - 0.095$.

The final values employed in the material card of the composite in the low velocity model were already shown in the manuscript but have also been included in this section Tab. 8.5.

T800/M21: Delamination Characterization

For the delamination characterization, the necessary experimental tests were also carried out in the reference study [25]. The process followed is explained on this part to give some

Failure ϵ / Ply Angle	Description	± 45 deg	90 deg	0 deg
ϵ_T^f DFAILT (%)	Fibre tension	2	0.6	1.557
ϵ_C^f DFAILC (%)	Fibre compression	-7	-3.3	-1.05
ϵ_M^f DFAILM (%)	Matrix tension/ compression	-7	3.3	1.05
ϵ_S^f DFAILS (%)	Shear	3.5	0	0

Table 8.5: Strains to failure parameters inside material formulation.

more detail on the experimental and numerical procedures that are necessary to compute these fracture mechanics parameters.

For the first delamination **mode I (opening)** the quasi-static double cantilever beam (DCB) tests were carried out according to ISO–15024 standard. Some crack gages were used to measure the variation in voltage when a crack propagates through them. The crack length, a , as a function of load point opening displacement σ is computed (5 to 15 mm). Then, an R-curve which shows the evolution of the energy release rate (fracture toughness) G_{Ic} as a function of the size of the crack a , thorough the DCB test is computed. Finally, for T800S/M21, one can consider that at a size of $a = 40 - 50$ mm the crack initiation occurs. The computed energy fracture toughness for mode I is $G_{Ic} = 765\text{J/m}^2$, the value used for numerical simulation of DCB and impact simulations of T800S/M21.

The second delamination **mode II (shear)** parameters were obtained from the end loaded split (ELS) tests carried out on a screw driven tension-compression machine. The R-curve for ELS tests is computed through the test results and a final value mode II toughness is reached $G_{IIc} = 1250\text{J/m}^2$. This value can be used for numerical simulations of impact problems.

The rest of the parameters involved in the tiebreak contact modelling are shown in the following table Tab. 8.6.

Contact Tiebreak Option/Parameters	Description	OPTION=7	OPTION=6	OPTION=9
NFLS	Normal failure stress (MPa)	60	60	60
SFLS	Shear failure stress (MPa)	60	60	60
PARAM	Friction angle, ϕ (rad) Critical distance, CCRIT (mm) Damage model exponent, α	0	0.025	1
ERATEN	Normal energy release rate (J/m^2)	765	765	765
ERATES	Shear energy release rate (J/m^2)	1250	1250	1250
CT2CN	Ratio tangential to normal stiffness	n/a	n/a	1
CN	Normal stiffness (kN/mm^3)	n/a	n/a	100

Table 8.6: Tiebreak contact options parameters definition and values implemented in the numerical model [25].

8.2.2 Rigid Projectile: Steel

The mechanical properties of the rigid steel projectile are shown in Tab. 8.7.

Mechanical Properties Steel	ρ (kg/m^3)	E (GPa)	ν
	7857	206.7	0.3

Table 8.7: Mechanical properties steel impactor high velocity impact model. [39]